7906 *Biochemistry* **2009,** *48,* 7906–7915
DOI: 10.1021/bi900084m

BIOCHEMISTRY
including biophysical chemistry & molecular biology
Article

The 1.85 Å Structure of an 8*R*-Lipoxygenase Suggests a General Model for Lipoxygenase Product Specificity[†]

David B. Neau,[§,⊥] Nathaniel C. Gilbert,[§] Sue G. Bartlett,[§] William Boeglin,[∥] Alan R. Brash,[∥] and Marcia E. Newcomer*[,§]

[§]*Department of Biological Sciences, Louisiana State University, Baton Rouge, Louisiana 70803, and* [∥]*Department of Pharmacology, Vanderbilt University School of Medicine, Nashville, Tennessee 37232.* [⊥]*Present address: NE-CAT/Cornell University, 9700 S. Cass Ave., Bldg. 436 E004, Argonne, IL 60439.*

Received January 20, 2009; Revised Manuscript Received July 13, 2009

ABSTRACT: Lipoxygenases (LOX) play pivotal roles in the biosynthesis of leukotrienes and other biologically active eicosanoids derived from arachidonic acid. A mechanistic understanding of substrate recognition, when lipoxygenases that recognize the same substrate generate different products, can be used to help guide the design of enzyme-specific inhibitors. We report here the 1.85 Å resolution structure of an 8*R*-lipoxygenase from *Plexaura homomalla*, an enzyme with a sequence ~40% identical to that of human 5-LOX. The structure reveals a U-shaped channel, defined by invariant amino acids, that would allow substrate access to the catalytic iron. We demonstrate that mutations within the channel significantly impact enzyme activity and propose a novel model for substrate binding potentially applicable to other members of this enzyme family.

Lipoxygenases are non-heme iron dioxygenases that catalyze the stereo- and regiospecific formation of fatty acid hydroperoxides from polyunsaturated fatty acids (*1*, *2*). In animals, lipoxygenases (LOX)[1] play pivotal roles in the biosynthesis of leukotrienes and other biologically active eicosanoids derived from arachidonic acid (AA). Consequently, the enzymes are targets for the development of specific inhibitors to modulate the physiological and pathological effects of the potent signaling compounds they generate (*3*, *4*). Because lipoxygenases are iron enzymes, they can be inhibited by iron chelators or redox active compounds. However, these modes of inhibition are inherently nonspecific. To engineer specificity into any inhibitor, more structural information for this enzyme family is required, yet no LOX structure provides a comprehensive model for how substrate binds in the active site, a model central to the development of isozyme-specific inhibitors. A mechanistic understanding of substrate recognition, in which lipoxygenases that recognize the same substrate discriminate among the three chemically equivalent carbons of arachidonic acid to generate different products, can be used to help guide the design of novel inhibitors. Work with the plant enzymes has afforded tremendous insight into the mechanism of hydrogen abstraction by the active site iron, but the basis for the specificity of oxygenation in LOX catalysis is still unclear (*5*).

We report here the 1.85 Å resolution structure of an 8*R*-lipoxygenase from *Plexaura homomalla*, an enzyme that, like human LOX isoforms, is ~40% identical in sequence to human 5-LOX, the enzyme that initiates leukotriene biosynthesis. The structure reveals a U-shaped channel, defined by invariant isoleucines and leucines, that allows substrate access to the catalytic iron. We demonstrate that mutations within this channel significantly impact enzyme activity. On the basis of our results, we propose a model for substrate binding in which an invariant Leu points into the U-shaped channel and restrains the targeted pentadiene for hydrogen abstraction. The register of the pentadiene positioned for attack is set by protein−substrate interactions at either end of the U-shaped channel.

The features of an 8*R*-LOX binding site must be able to account for the regio- and stereospecificity of the enzyme yet exhibit the potential flexibility to explain the range of specificities found within the LOX enzyme superfamily. Consequently, the model must be compatible with several well-established aspects of LOX catalysis. (i) The non-heme iron, positioned by amino acids that fill five of the six sites of the coordination sphere, interacts with the substrate via its sixth position as Fe^{3+}-OH. Sequence, structural, and biochemical data suggest that the geometry of the catalytic machinery is conserved among LOX enzymes. (ii) Fe^{3+}-OH initiates catalysis by stereoselective removal of one hydrogen from the CH_2 group in a *cis*-CH_2-*cis* double bond unit (pentadiene) of the substrate. The free radical pentadiene intermediate generated by H abstraction is oxygenated on its opposite face, at one of two possible positions (+2 or −2 carbon). Reaction at the +2 or −2 position yields products of opposite stereochemistry (*R* or *S*, respectively) (Figure 1). (iii) A conserved active site Gly in *R*-LOX is associated with *R* oxygenation. Its counterpart in *S*-LOX is Ala. A Gly−Ala switch by mutagenesis redirects oxygenation across the face of the pentadiene, changing the positional specificity along with *R* or *S* stereochemistry. (iv) The fatty acid substrate is held in one head-to-tail orientation or the other. While four distinct hydroperoxide products can arise from each pentadiene in the substrate, each LOX generates

[†]This work was supported in part by the National Science Foundation (MCB-0818387), the American Heart Association (0855392E), and the Louisiana Governor's Biotechnology Initiative (to M.E.N.) and the National Institutes of Health (Grants GM 74888 and GM 15431 to A.R.B.).

*To whom correspondence should be addressed: Department of Biological Sciences, Louisiana State University, Baton Rouge, LA 70803. Telephone: (225) 578-7383. Fax: (225) 578-7258. E-mail: newcomer@lsu.edu.

[1]Abbreviations: AA, arachidonic acid; LOX, lipoxygenase(s); 8*R*-HPETE, 8*R*-hydroperoxyeicosatetraenoic acid; PDB, Protein Data Bank; RP-HPLC, reversed phase high-pressure chromatography.

 Published on Web 07/13/2009

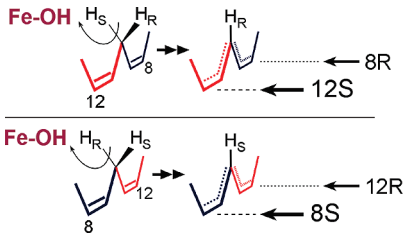

FIGURE 1: Regio- and stereospecificity in lipoxygenases. Relationship of iron-catalyzed hydrogen abstraction and oxygenation on the opposite face of the reacting substrate. In the top panel, with arachidonic acid in this head-to-tail orientation, abstraction of 10-H_S (pro-*S*) gives either 8*R* or 12*S* oxygenation products. In the bottom panel, 10-H_R (pro-*R*) abstraction leads to 8*S* or 12*R* products.

only a single specific product. For example, LOX-catalyzed peroxidation of the central pentadiene of arachidonic acid requires hydrogen abstraction at C10 and could potentially generate 8*R* or 12*S* with AA bound in one orientation, and 8*S* or 12*R* with AA bound in the inverse orientation (Figure 1). For the enzyme described herein, only the 8*R* product is observed. (v) Finally, some lipoxygenases produce the identical hydroperoxide product from free arachidonic or linoleic acids or their large esters (e.g., phospholipid esters). This implies that the carboxyl group does not enter the active site; thus, the binding orientation for these enzymes (e.g., 15*S*-LOX) has generally been designated as "tail first" into the active site. In contrast, the 5*S*, 8*S*, or 12*R* enzymes cannot oxygenate the phospholipid esters, and their product specificities can be explained by "head-first" entry into the active site. There are, however, notable exceptions to this last rule which require a rational explanation as we discuss later.

In effect, active site control of LOX product specificity is determined by three factors: which pentadiene of the substrate is positioned for attack, whether the pro-*R* or pro-*S* hydrogen of the pentadiene is positioned for abstraction, and whether O_2 has access to C_{-2} or C_{+2}. Our model provides a structural framework for understanding the determinants of product diversity of lipoxygenases.

MATERIALS AND METHODS

Protein Crystallization. A deletion mutant of *P. homomalla* 8*R*-LOX engineered for improved solubility, here termed pseudo-wild type (pSWT), was concentrated to ~10 mg/mL and crystallized by sitting drop vapor diffusion as previously reported (*6*). The I433W and I433A mutants of psWT were constructed using whole plasmid polymerase chain reaction. I433W·psWT and I433A·psWT crystals were obtained by sitting drop vapor diffusion in 5−8% PEG 8000, 5% glycerol, 0.2 M $CaCl_2$, and 0.1 M imidazole acetate (pH 8.0). Crystallizations were performed in a Coy anaerobic chamber. The crystals, which grew overnight, were mounted using a cryo-protecting solution of 10% PEG 8000, 25% glycerol, 0.02 M $CaCl_2$, and 0.1 M imidazole acetate (pH 8.0).

X-ray Data Collection and Structure Determination. X-ray diffraction data (psWT, I433W·psWT, and I433A·psWT) were collected at the Gulf Coast Protein Crystallography Consortium beamline at the Center for Advanced Microstructures and Devices (CAMD, Louisiana State University) using 1.38 Å radiation at a temperature of 100 K. Data for psWT, I433W·psWT, and I433A·psWT were processed to a resolution of 1.85, 1.9, and 2.3 Å, respectively (Table 1), using the HKL2000 package (*7*). The structure of psWT was determined by molecular replacement using the previously published 3.2 Å structure of coral 8*R*-lipoxygenase (PDB entry 2FNQ) (*8*). The two mutant structures were determined by using only the protein atoms from the refined parent structure as a starting model, refining the protein model and adding ions, small molecules, and waters. Model building was done with Coot (*9*) and refinement with REFMAC5 (*10*)and Phenix (*11*). Model quality was assessed using MolProbity (*12*). For the psWT structure, 97% of the residues are in the favored region of the Ramachandran plot, with only a single residue outside the allowed region out of 2800 total residues (there are four molecules in the asymmetric unit). The I433W·psWT structure had 96.9% of the residues in the favored region of the Ramachandran plot, with only one outside the allowed region out of 2810 residues. The I433A·psWT structure had 96.7% of the residues in the favored region of the Ramachandran plot, with four residues outside the allowed region out of 2758 residues.

Enzyme Kinetics. The LOX activity assay of wild-type 8*R*-LOX and its mutants was conducted in a 1 mL sample volume [in 50 mM Tris buffer (pH 7.5) and 150 mM NaCl] by following the absorbance increase at 235 nm due to the formation of the conjugated diene chromophore using a Lambda 35 UV−vis spectrophotometer (PerkinElmer). The concentration of the wild-type enzyme was 12.5 nM; for the less active mutants, enzyme concentrations were increased up to 63 nM. The substrate concentration was varied from 10 to 200 μM. The rates of reaction were calculated from the initial linear part of the curve. Values for K_m and turnover were determined by nonlinear regression analysis of a plot of velocity versus substrate concentration data to the Michaelis−Menten equation. Activity for the I433A·psWT enzyme was only measurable in the presence of detergent and $CaCl_2$ [50 mM Tris (pH 7.5), 500 mM NaCl, 0.05% emolphogen, and 2 mM $CaCl_2$].

Product Analysis. 8*R*-Lipoxygenase mutagenesis was performed using the Stratagene Quickchange mutagenesis kit according to the manufacturer's instructions to replace Leu-432 with Ala, Val, Ile, or Phe. Expression and purification of the wild type, psWT, and all mutants for product analysis was performed as reported by Boutard et al. (*13*). Protein was quantified by running on a 20 to 4% polyacrylamide gel along with a series of known amounts (1−10 μg) of BSA as previously described (*14*). Incubations were conducted in 50 mM Tris (pH 8.0) containing 500 mM NaCl, 2 mM $CaCl_2$, and 0.05% Emulphogen (Sigma) with 50 μM arachidonic acid containing 5×10^5 cpm of [1-^{14}C]-arachidonic acid. Samples were incubated for 10 min at room temperature (with shaking), subsequently extracted with a Waters 1 cm^3 Oasis HLB cartridge, and eluted with 1 mL of methanol. Treatment with triphenylphosphine in methanol at room temperature for 10 min was performed to reduce the hydroperoxyeicosatetraenoic acids (HPETEs) to their hydroxy counterparts (HETEs).

Samples were analyzed initially by RP-HPLC using a Waters Symmetry C18 column (250 mm × 4.6 mm) with a methanol/water/glacial acetic acid solvent system (80:20:0.01, by volume) running at 1 mL/min. The eluant was monitored with an Agilent 1100 diode array detector in series with a Radiomatic Flo-One/Beta A100 inline scintillation counter. This allowed determination of the conversion of substrate to H(P)ETEs (8- and 12-HETE are not well resolved on this system; they elute close together, partly resolved with 12-HETE eluting before 8-HETE).

Table 1: Data Collection and Refinement Statistics

	psWT	I433W·psWT	I433A·psWT
		Data Collection	
space group	$P2_1$	$P2_1$	$P2_1$
cell dimensions			
a, *b*, *c* (Å)	103.98, 170.22, 104.50	103.70, 170.21, 104.90	104.36, 170.38, 104.90
α, *β*, *γ* (deg)	90, 95.88, 90	90, 95.51, 90	90, 95.51, 90
resolution (Å)	30−1.85	50−1.90	30−2.30
R_{sym} [a]	0.068 (0.677)[b]	0.086 (0.693)[b]	0.124 (0.660)[b]
$I/\sigma I$	21.0 (2.32)[b]	17.1 (2.31)[b]	12.8 (2.27)[b]
completeness (%)	98.8 (98.0)[b]	98.6 (100)[b]	100 (100)[b]
redundancy	4.0 (4.0)[b]	4.9 (5.1)[b]	4.9 (4.7)[b]
		Refinement	
resolution (Å)	30−1.85	35−1.90	30−2.30
no. of reflections	287452	263905	150209
R_{work}/R_{free} [c]	0.1740/0.2093	0.1591/0.2037	0.1675/0.2389
no. of atoms			
protein	22141	22299	21805
ligand			34
ion/glycerol/acetate	284	250	224
water	2667	2485	1582
B-factor (Å^2)			
protein	26	27.48	27.99
ligand			43.37
ion/glycerol/acetate	35.68	38.13	38.8
water	37.26	38.31	30.84
root-mean-square deviation			
bond lengths (Å)	0.015	0.016	0.023
bond angles (deg)	1.409	1.5	1.94

[a] $R_{merge} = \sum|I_i - \langle I\rangle|/\sum I_i$, where I_i is the intensity of the *i*th observation and $\langle I\rangle$is the mean intensity of the reflection. [b] Values in parentheses are for the highest-resolution shell. [c] $R = \sum||F_o|-|F_c||/\sum|F_o|$, where F_o and F_c are the observed and calculated structure factor amplitudes, respectively. R_{free} was calculated using 5% of the total reflections.

The samples were then methylated using diazomethane, and the relative amounts of the individual HETE methyl esters (8- and 12-HETE) were determined via normal phase HPLC using a Beckman Ultrasphere Si column (4.6 mm × 250 mm) in hexane and 2-propanol (100:1, v/v) at 1 mL/min. The chiralities of the 8-HETE and 12-HETE methyl ester products were analyzed using a Chiralpak AD column (250 mm×4.6 mm) using a hexane/methanol solvent (100:2, v/v) at 1 mL/min (*15*). Sample chromatograms are provided in Figure S1 of the Supporting Information.

RESULTS

High-Resolution 8R-LOX Structure. 8*R*-LOX crystals diffracting to 1.85 Å were obtained following modifications to a putative membrane insertion loop and calcium binding sites as detailed elsewhere (*6*). The modified protein crystallized in space group $P2_1$ with four molecules in the asymmetric unit. The structure of the mutant protein (Figure 2) confirmed the supposition that removal of the putative membrane insertion loop and calcium binding amino acids has no structural consequences outside the immediate vicinity of the deletion. For the psWT structure, 97% of the residues are in the favored region of the Ramachandran plot, with only a single residue outside the allowed (including the generously allowed) regions (of 2800 total residues; four molecules in the asymmetric unit). The I433W·psWT structure had 96.9% of the residues in the favored region of the Ramachandran plot, with only one outside the allowed regions (of 2810 residues). The I433A·psWT structure had 96.7% of the residues in the favored region of the Ramachandran plot, with four residues outside the allowed regions (of 2758 residues).

The average main chain *B*-factors in the region of the mutations (429−441) are elevated in all three structures. This segment corresponds to a surface-exposed helix that shelters a large solvent-filled channel, as described below. Electron density is clear for the main chain of both the psWT and I433W·psWT forms, but not necessarily for the full length of the solvent-exposed side chains. In contrast, unbroken main chain electron density for the I433A·psWT backbone in this region is not observed. For both the pseudo-wild-type and I433A structures, the average main chain *B*-factors in the segment from position 429 to 441 are twice that for the overall main chain (average main chain temperature factors of 21.0 and 23.5 Å^2, respectively; Wilson *B*-factors of 24.9 and 34.9 Å^2, respectively). In contrast, the average main chain temperature factor for residues 429−441 in I433W·psWT is only 50% higher than the overall main chain *B*-factor (average main chain value of 22.7 Å^2; Wilson *B*-factor of 26.3 Å^2). The elevated temperature factors are consistent with the fact that the helical region is surrounded by solvent in all four molecules in the asymmetric units in each of the structures.

Lipoxygenases contain an N-terminal C2-like domain (~110 amino acids) and a predominately helical domain (~550 amino acids in animal lipoxygenases) in which the catalytic Fe is ligated by amino acid side chains and the main chain carboxylate of the C-terminal amino acid. 8*R*-LOX has three Ca^{2+} binding sites flanked by putative membrane insertion loops in the C2-like

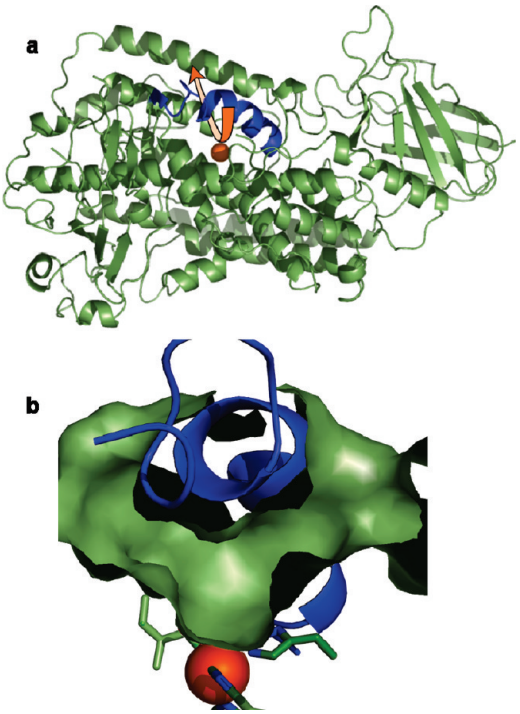

FIGURE 2: Structure of psWT, a soluble form of 8*R*-LOX. (a) Cartoon rendering of the enzyme. The arched helix that shelters the catalytic Fe (orange sphere) is colored blue. An orange arrow indicates the location of the U-shaped channel. (b) Cross section of the U-shaped channel which passes under the arched helix. These renderings were generated with PyMOL(*43*) and CastP (*44*).

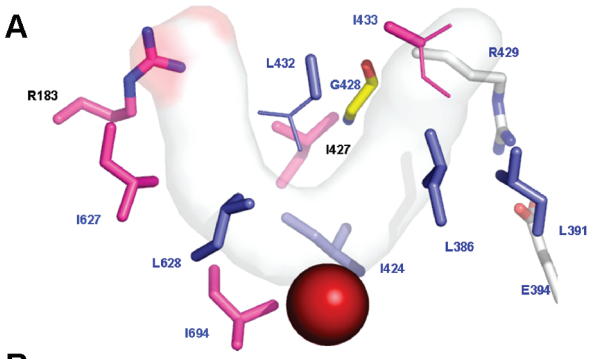

B

8R-LOX	LLQPHIYGVLAIDTIGRKELIGSGGIVDQSLSLGGGGHVTFMEK	456
Q5DWF4_9CNID	LLQPHIYGVLAIDTIGRKELIGSGGIVDKSLSLGGGGHVEFMEK	430
Q2N410_9CNID	LLYPHTKGIMAINTLGRNDLIPTGGAADKVLSIGGGGQVTLMQK	400
Q4RJE8_TETNG	LLIPHTRYTLQINLLARIRLISETGVFSKFTASGGEGMLSILKK	320
LOX15_HUMAN	LIIPHLRYTLEINVRARTGLVSDMGIFDQIMSTGGGGHVQLLKQ	326
LOX15_PONPY	LIIPHLRYTLEINVRARTGLVSDMGIFDQIMSTGGGGHVQLLKQ	326
LOX12_BOVIN	LLIPHLRYTMEINIRARTGLVSDSGVFDQVVSTGGGGHVELLQR	326
LOX12_PIG	LLIPHFRYTMEINVRARNGLVSDLGIFDQVVSTGGGGHVELLRR	326
LOX15_RABIT	LIVPHLRYTLEINVRARNGLVSDFGIFDQIMSTGGGGHVQLLQQ	326
LX12L_RAT	LLVPHLLYTMEINVRARSDLISERGFFDKAMSTGGGGHLDLLKQ	326
LX12L_MOUSE	LLVPHLLYTMEINVRARSDLISERGFFDKVMSTGGGGHLDLLKQ	325
LOX12_HUMAN	FLIPHIRYTMEINTRARTQLISDGGIFDKAVSTGGGGHVQLLRR	329
Q95103_BOVIN	LLMPHIRYTMEINTRARTQLISDGGIFDKAVSTGGGGHVHLLRR	295
LOX12_MOUSE	LLVPHIRYTMEINTRSRTQLISDGGIFDQVVSTGGGGHVQLLTR	329
Q7T2A9_DANRE	LLTPHLRYTLEINCRGRTQLLSPEGIFKRVVSTGGEGLLILAQR	392
LOX5_RAT	LLVAHVRFTIAINTKAREQLNCEYGLFDKANATGGGGHVQMVQR	392
LOX5_MOUSE	LLVAHVRFTIAINTKAREQLICEYGLFDKANATGGGGHVQMVQR	399
LOX5_MESAU	LLVAHVRFTIAINTKAREQLICEYGLFDKANATGGGGHVQMVQR	398
LOX5_HUMAN	LLVAHVRFTIAINTKAREQLICECGLFDKANATGGGGHVQMVQR	400
A0JM77_XENTR	LLIAHVRFTIAINTKAREQLICECGLFDKANATGGGGHVELLLR	284
Q503R7_DANRE	LLIPHVRFTIAINTSARQTLINDTGVFNKANSTGGIGVLQVVHR	325
LOX1_ AT	LLEPHFRDTMNINALARQILINGGGIFEITVFPSKYA-MEMSSF	589
L1_SOYBEAN	LLTPHVRNMMNINALARQSLINANGIIETTFLPSKYS-VEMSSA	571
LOXA_TOMATO	LLYPHFRDTMNINALARQILINAGGVLESTVFPSKFA-MEMSAV	591

FIGURE 3: Proposed AA binding site in 8*R*-LOX. (a) A modeled arachidonic acid in the proposed 8*R*-LOX active site. The site is lined with Leu and Ile side chains. The side chains of L432 and I433 are not visible in the electron density map, and the thinner stick rendering corresponds to the most favored rotamer for these amino acids. Side chains identified by Evolutionary Trace (*22*) as invariant are colored blue, while both invariant and highly conserved resides are numbered in blue text. The only residues unique to the 8*R* enzyme are R183 and I427. The backbone of G428 is included in stick rendering (C, yellow; O, red; N, blue), and the conserved salt link in which R429 participates is depicted (C, white; O, red; N, blue). A modeled AA is rendered as a transparent surface (C, white; O, red). (b) A partial sequence alignment of lipoxygenases. I424 and L432, which line the putative recognition site, are invariant, while I433 is highly conserved. R429 is part of the invariant salt link that anchors the arched helix to the catalytic core. The conserved G localized in the arch of the helix is colored red. Taxonomic identifiers: 9CNID, *Cnidaria*; RAT, *Rattus norvegicus*; TETNG, *Tetraodon nigroviridis*; HUMAN, *Homo sapiens*; PONPY, *Pongo abelii*; BOVIN, *Bos taurus*; PIG, *Sus scrofa*; RABIT, *Oryctolagus cuniculus*; MOUSE, *Mus musculus*; DANRE, *Danio rerio*; MESAU, *Mesocricetus auratus*; XENTRO, *Xenopus tropicalis*; AT, *Arabidopsis thaliana*; SOYBEAN, *Glycine max*; TOMATO, *Lycopersicon esculentum*.

domain, and the deletion mutant used in these studies lacks one of the loops, as well as chelating amino acids from two of the three Ca^{2+} binding sites (the center site and that most distal from the catalytic domain). The Ca^{2+} site proximal to the catalytic domain, defined primarily by main chain contacts, remains intact and occupied in the mutant structure. Additional density which may be a Ca^{2+} ion is associated with E52, but the coordination sphere of the heptacoordinated ion contains only two protein atoms, and these from different molecules, and is not likely a biologically relevant interaction. Ca^{2+} promotes the binding of 8*R*-LOX to membranes (*8*). The deletion mutant displays wild-type activity in a membrane-free assay; however, Ca^{2+} does not promote membrane binding of the mutant and does not stimulate enzyme activity in a membrane-based assay. Thus, we refer to this enzyme as the pseudo-wild type (psWT) in accordance with its nativelike structure and catalytic activity in the absence of membranes.

The Structure Reveals a Channel with Conserved Features. A striking feature of the electron density map obtained for psWT is a U-shaped channel, open at both ends, which runs under an arched helix and allows access to the catalytic iron from two directions. The channel is a culvert which runs underneath the arch provided by the curvature of α9, roughly orthogonal to it (Figure 2). At the apex of the arch, sheltering the culvert, is the helical turn that includes residues 428−432. From this turn, the side chain of L432 points down into the U-shaped channel. At the base of this U-shaped channel sits the catalytic iron. This arched, or discontinuous, helix [in *P. homomalla* α9−10 (Figure S2 of the Supporting Information)] is found in all available lipoxygenase structures (*16*−*21*). The discontinuity is a consequence of a reverse turn insertion previously discussed by Minor et al. (*17*). The insertion, which corresponds to the highly conserved glycine (Figure 3) in animal and plant LOX, has the effect of creating a long, curved helix that arches away from the bundle of helices that constitute the catalytic domain. The C-terminal end of the helix is anchored to the LOX body by a salt link between R429 on α9 and E394 on α7 [8*R*-LOX numbering (Figure S2 of the Supporting Information)]. Both the Arg and Glu that make the salt link are conserved in almost all available lipoxygenase sequences.

In the electron density map, the U-shaped channel is deceptively large since the side chains of I433 and L432 are not visible, an indication of either static or dynamic disorder. However, even when the volume of the side chains of these amino acids is taken into account, there is room for AA to slide into the channel and

position C10 of the central pentadiene for attack. Positively charged residues, R183 and R429, that could neutralize the carboxylate of AA are located on both sides of the channel. Since R429 participates in the invariant salt link described above, anchoring the arched helix (the roof of the channel) to the helical cluster that forms the catalytic domain, it is more likely that R183 is the neutralizing residue that positions the substrate in 8*R*-LOX for attack at C10. Lipoxygenases that vary with respect to positional specificity would be expected also to vary with respect to the positions of their substrate tethering amino acids. In contrast, the environment that surrounds the pentadiene for H abstraction is likely to be conserved.

Site-Directed Mutagenesis of the Amino Acids Lining the Channel. L432, which points into the culvert and is positioned above the catalytic iron (Figure 3), is fully solvent exposed and has no side chain density past C_β. There is, however, sufficient space between a Leu side chain and the catalytic iron for the Leu to secure the pentadiene for hydrogen abstraction by Fe^{3+}-OH. L432 is invariant in the lipoxygenase sequences available from plants, animals, and microorganisms. A role in positioning the pentadiene for attack is consistent with this pattern of conservation. The alternative interpretation, that the Leu is conserved because it plays an important role in the stabilization of the common structural framework, is difficult to reconcile with the fact that the amino acid is both solvent-exposed and highly mobile, properties not generally associated with structurally important amino acids.

To investigate a functional role for L432, mutant enzymes with conservative substitutions were constructed by replacement of L432 with Ala, Val, Ile, or Phe. The Ala, Ile, and Phe mutations produced enzyme with $<5\%$ of the activity of the wild-type enzyme. While the effect of Val was less dramatic, L432V·8*R*-LOX still displays $<20\%$ of the wild-type activity. According to the results of kinetic experiments, this loss of activity cannot be attributed to a loss of affinity for the substrate, as the K_m for AA for the mutant enzymes is not significantly changed from that of psWT (Table 2). Rather, the mutant enzymes have greatly reduced turnover numbers. These data support a role in catalysis for L432. In addition, approximately one-third of the L432F product is 12*S* rather than 8*R*; thus, both the specificity and the rate of reaction are compromised with this mutation. These results combine to suggest that L432 plays a role in positioning and restraining the substrate pentadiene. The reduced rates of reaction and altered product profiles can be a consequence of the pentadiene being improperly positioned for H abstraction and/or ineffectively restrained for oxygenation.

I433 mutants (I433A and I433W), a second channel-lining amino acid for which no electron density is visible past C_β, were prepared in the background of the psWT. The structures of the mutated enzymes were determined, and the effects of the mutations on catalytic activity were evaluated. Both mutations greatly impair enzyme activity; no activity for the I433W mutant is detected, and I433A·psWT has measurable activity only in the presence of $CaCl_2$ and the detergent emolphogen.

The crystal structures of the I433W and I433A mutant enzymes confirm that the only structural differences induced by the mutations are localized to the immediate vicinity of the amino acid substitution (Figure 4). However, the two substitutions have opposite effects: the side chains of the arched helix in the I433W·psWT structure are more ordered, while substitution with an Ala at the same position results in disordering of the helix main chain. In the I433W mutant, there is clear density for the Trp side chain (Figure 5) and it appears immobilized in the U-shaped site, partially filling an otherwise solvent exposed hydrophobic channel. The bulky Trp occupies space required for the AA tail according to our model. In addition, the side chain of L432 is clearly visible in the I433W electron density map and therefore no longer mobile. The replacement of I433 with a Trp appears to stabilize L432 and plug the tail end of the proposed AA binding site. This mutant has no measurable activity, presumably because the Trp side chain has effectively blocked the AA binding site.

Table 2: Mutagenesis

	Activity	
enzyme	K_m (μM)	turnover (s^{-1})
WT	50 ± 5	206 ± 8
L432A	33 ± 12	12 ± 1
L432F	–	trace of activity
L432I	18 ± 4	7 ± 1
L432V	28 ± 6	42 ± 3
I433A·psWT[a]	135 ± 4	19 ± 3
I443W·psWT	nd[b]	nd[b]

	Regiospecificity	
enzyme	12 (%)	8 (%)
WT	2	98
L432A	10	90
L432F	34	66
L432I	3	97
L432V	1	99
I433A·psWT	11	89

	Stereochemistry			
enzyme	8*R* (%)	8*S* (%)	12*R* (%)	12*S* (%)
WT	100	0	10	90
L432A	99	1	3	97
L432F	95	5	7	94
L432I	99	1	8	92
L432V	100	0	–	–
I433A·psWT	95	5	16	84

[a] Assay conditions include 0.05% emolphogen and 2 mM $CaCl_2$. [b] Not detected.

In contrast, in the I433A mutant, the helical arch which spans the culvert in the wild-type enzyme is not fully defined in the electron density map: there is no density for side chains or backbone from residue 432 to 436. It appears that the absence of the Ile side chain has destabilized the "roof" of the U-shaped channel. This destabilization negatively impacts the catalytic capacity of the enzyme since L432, a critical side chain according to the results described above, is one of the residues destabilized by the mutation. This mutant produces predominantly the 8*R* product, but at a significantly impaired rate (Table 2).

Thus, mutation of amino acids that line the U-shaped channel significantly impact catalytic activity. More importantly, the crystal structures confirm that amino acid substitutions in this region have no structural impact outside the immediate vicinity of the mutated region. Since both L432 and I433 are mobile and solvent-exposed in the pseudo-wild-type structure, a structural role for these amino acids is unlikely. The observation that substitutions have such a dramatic effect on enzyme activity is

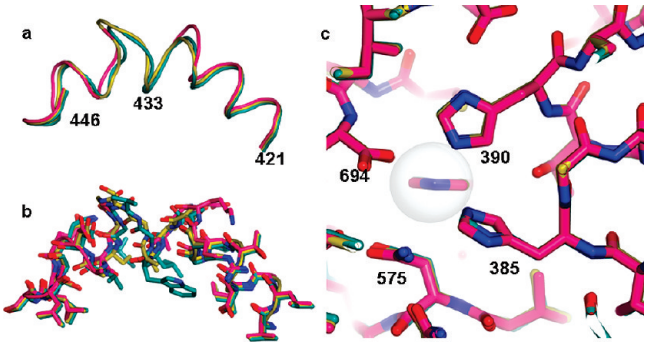

FIGURE 4: Superposition of psWT, I433W·psWT, and I433A·psWT. (a) Ribbon overlay of arched helices. There is no density for amino acids 432−436 in the I433A·psWT structure (psWT, gold; I433W·psWT, teal; I433A·psWT, pink). (b) Detail of the arched helix. (c) The overlay of the active sites reveals no structural differences among the mutants. Fe is shown as a transparent sphere.

consistent with functional roles, such as substrate positioning, for these amino acids.

The AA binding site we propose (Figure 3) based on the 1.85 Å 8*R*-LOX structure is lined with invariant amino acids in the immediate vicinity of the site that accommodates the pentadiene. In support of our experimental results, when Evolutionary Trace (*22*−*24*) is employed to visualize patterns of sequence conservation in lipoxygenases in a three-dimensional context, five hydrophobic amino acids lining the U-shaped channel are strictly conserved in arachidonate-metabolizing lipoxygenases: Leu-386, -391, -432, and -628 and Ile-424. The amino acids that set the register of the AA and dictate which pentadiene is available for H abstraction should flank this area. Since LOX isoforms produce a wide array of products, little conservation of flanking amino acids that bind the carboxylate and tail ends of AA is predicted. Indeed, there is a lack of sequence conservation among lipoxygenases in these regions.

DISCUSSION

The U-Shaped Channel Contrasted with the Previously Described "Boot-Shaped" Cavity. Prior to our work, the only animal LOX structure available was that of rabbit reticulocyte 15-LOX in complex with the inhibitor RS7 (*18*). Since both the U-shaped channel and the boot-shaped cavity of the rabbit 15-LOX structure must provide a path for the pentadiene to approach the catalytic iron, there is overlap between the predicted substrate binding sites. In the two lipoxygenase models, the essential difference is that the boot-shaped cavity protrudes past the Fe and deeper into the enzyme, whereas the U-shaped site veers back up toward the surface. An illustration of the amino acid side chains that define the two sites is rendered in Figure 6. F353 in 15-LOX is proposed to form the floor of the substrate binding site, with the bulky amino acid precluding further penetration of the AA tail. There is a similarly positioned internal cavity in the 8*R* structure, but it is appreciably smaller in volume. However, according to the 15-LOX-derived model (*25*), the cavity should be larger in 8*R*-LOX since the AA must enter three carbons deeper to allow the positioning of C10, rather than C13, at the iron coordination sphere. The positional specificity of the 8*R* enzyme is inconsistent with a smaller volume of this cavity. In contrast, the volume and details of the U-shaped channel are consistent with a role in AA binding. The U-shaped channel is defined by the side chains of five Leu and four Ile residues and displays a remarkably high degree of sequence conservation (seven invariant/highly conserved in animal lipoxygenases). While there are site-directed mutagenesis data that support the boot-shaped cavity (*18*, *25*, *26*), some do not (*27*). Moreover, in no case are structural data presented to evaluate the impact of the mutations on enzyme structure. While some results may be compatible with that model, an alternative such as the U-shaped channel cannot necessarily be ruled out.

Partial overlap of substrate and inhibitor binding sites, as a consequence of the structural adaptability of the ligand binding pocket, has previously been described for the structures of the ecdysone receptor in complex with a hormone or antagonist (*28*). The details of the 15-LOX·RS7 structure suggest that as was case for the ecdysone receptor, the inhibitor is sufficiently dissimilar in structure from the natural substrate that it is not a true substrate/ligand mimic. In the case of the 15-LOX·RS7 structure, two major stabilizing forces of the protein−ligand interaction (charge−charge and aromatic−aromatic) are not relevant to the natural substrate. First, the carboxylate of the inhibitor is neutralized by the catalytic non-heme Fe, limiting access to the space the pentadiene must occupy for H abstraction to occur. Second, the aromatic ring of the inhibitor, which has no counterpart in the natural substrate, is buried deep in an aromatic cluster. Thus, it may be that the 15-LOX inhibitor does not fully define the substrate binding cavity.

The recent results of photoaffinity labeling of the active site of 15-LOX are readily explained with our U-shaped cavity extrapolated to that enzyme (*29*). Photoaffinity substrate analogues with a reactive azido group at the methyl end were cross-linked to two peptides in 15-LOX. Only one peptide contains amino acids shown to be important for AA binding and consistent with the boot-shaped cavity model (I593) (*25*). In contrast, when our proposed AA binding site is modeled in 15-LOX, the binding site is flanked by the two cross-linked peptides (Figure 6b). Specifically, the 15-LOX counterparts of amino acids I627 and L628 are provided by one of the peptides, while the other includes amino acids that plug the "back door" of our channel in the 15-LOX structure (W145 and K146). Importantly, while the U-shaped channel appears to be open at both ends in the 8*R*-LOX structure, this need not be the case for other LOX isoforms. The 15-LOX structure vividly illustrates this point. While a similar channel is apparent in the 15-LOX structure described by Choi et al. (*21*), the channel is closed by the presence of W145 and a salt link (K145 and D411) at one end. This closing and consequent shortening of the channel is consistent with the fact that AA need not penetrate as deeply into 15-LOX to position C13, rather than C10, for attack.

Comparison with Soybean Lipoxygenase L-1. As a rule, plant LOX enzymes are ~15−25 kDa larger than animal enzymes, utilize linoleic or linolenic acid (rather than AA) as a substrate, and share <25% sequence identity with animal LOX. The lipoxygenase core represented by the animal enzyme structures defines the core structure common to all lipoxygenases. Given the similarities in terms of both protein fold and catalytic machinery of animal and plant LOX, a model that provides a basis for product specificity in animal enzymes should also be relevant to the plant enzymes. Currently, there are X-ray crystal structures for soybean LOX L-1 (*16*, *17*, *30*), which is a 13-LOX with linoleic acid and a 15-LOX with arachidonic acid, and soybean LOX L-3 (*19*), which catalyzes nonspecific oxygenation of fatty acids and their esters, as well as two vegetative forms from soybean (*20*). There is no structure for a linoleate 9-LOX, an enzyme predicted to hold the substrate in the opposite head-to-tail

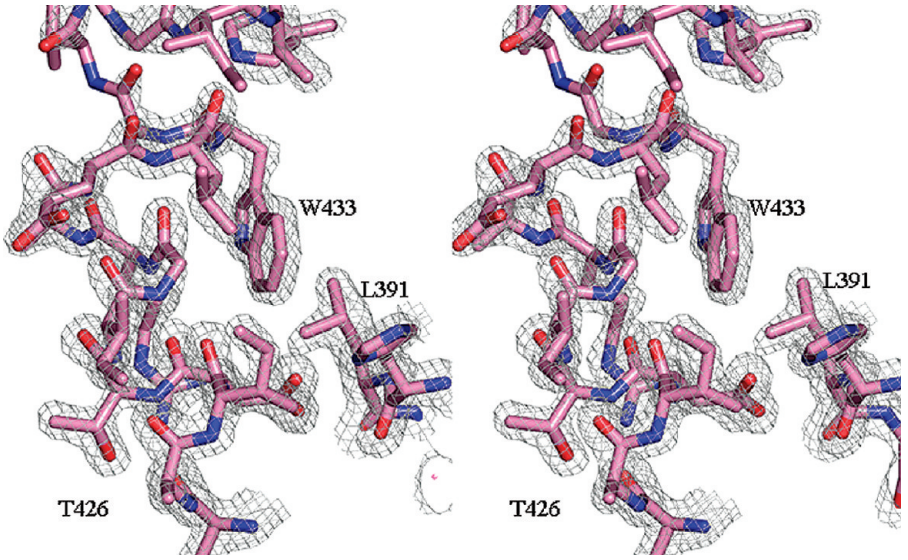

FIGURE 5: Portion of an electron density map. Stereorendering of the region of the Trp for Ile substitution in the 1.9 Å $2F_o-F_c$ electron density map of I433W·psWT, contoured at 2.0σ.

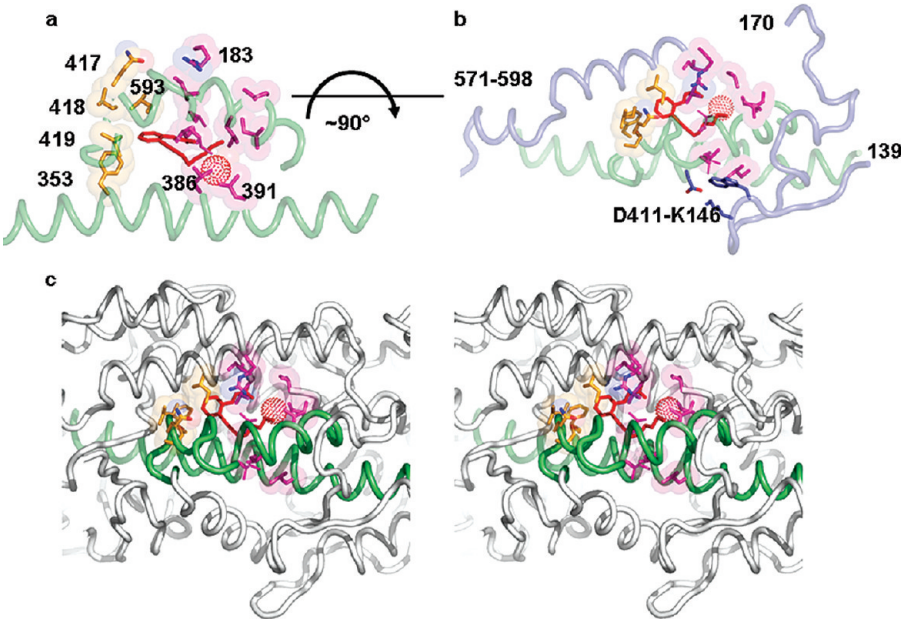

FIGURE 6: Comparison of the boot-shaped and U-shaped sites for AA binding. (a) Amino acids that line the proposed 15-LOX (orange) and 8*R*-LOX (pink) sites. The helical arch (421−441) and helix that includes residues 367−401 are shown in tube rendering. The RS7 inhibitor which defines the rabbit site is shown as a red stick and the iron as a dotted sphere. (b) This view is rotated ~90° about the *x*-axis. Included in tube rendering (blue) are the 15-LOX peptides that have been reported to cross-link with a photoreactive substrate analogue. Note that one of these peptides includes W145 and K145, amino acids which together with D411 (blue stick) plug the methyl end of the channel in 15-LOX. No amino acids from this peptide line the proposed 15-LOX binding site. (c) Stereoview of the context of the two cavities. The view is similar to that in panel b and looking from above the enzyme as rendered in Figure 2a.

orientation (*31*). The amino acids that envelop the pentadiene for attack in our model (L432, L628, and I424) are conserved in the plant enzymes, while the counterparts of L386 and L391 are substituted with Trp and Ala, respectively, in the plant enzymes. Although Trp narrows the channel, the accompanying substitution of Ala for Leu appears to compensate for this loss in volume. Klinman and co-workers (*32*, *33*) have proposed that Leu-546 and Leu-754, the plant counterparts to Leu-432 and Leu-628, respectively, are shielding amino acids in soybean LOX L-1. More recently, Meyer et. al mutated I553 and found that conservative mutations dramatically affected enzyme activity (*34*). I553 corresponds to V439 in 8*R*-LOX. This amino acid is positioned at the C-terminal end of the arch that shelters the U-shaped channel and in our model is a peripheral channel amino acid that helps define the substrate binding cavity.

While there is not a channel per se apparent in the soybean LOX structure, there is a cavity that can be accessed with a nominal conformational change. Furthermore, a subcavity which has been described as the O_2 access channel [illustrated in various plant LOX structures in a recent report (*20*)] appears to overlap with our U-shaped channel. The cavity does not have access to solvent as the additional polypeptide in the plant enzymes (relative to animal lipoxygenases) forms a β-hairpin that blocks channel access from what would correspond to the

methyl end (the back door) in our model, and the carboxyl end of the putative channel is blocked by the placement of the counterpart of helix α2. Minor et al. (*17*) previously suggested that T259, the counterpart of R183 on α2 in 8*R*-LOX, can be moved to allow entry into the active site cavity. Helix α2 is the only helix in the LOX core that has been described in differing positions in various LOX structures (*20*, *21*), and this conformational variability is consistent with the suggestion that a repositioning of this element of secondary structure could allow entry into the internal cavity. Alternatively, access via the back door of the channel would require the movement of a β-hairpin common to the plant enzymes. There is ample precedent for such a conformational change, and it would not require the repositioning of additional structural elements. Thus, one can envision tail-first entry from one of two possible ends of a substrate binding site that runs under the conserved arched helix in the plant enzymes as well.

An Explanation for Apparently Anomalous Substrate Specificities. The boot-shaped cavity model imposes a major constraint on the physical size of substrates that could bind in the reverse orientation as it requires that the carboxyl group be innermost in the binding cavity. When the fatty acid substrates are provided as the corresponding esters, the internal cavity needs to accommodate a bulkier headgroup. Indeed, this criterion has been used in support of so-called tail (methyl end)-first versus head (carboxyl end)-first entry of substrate into the active site. LOX enzymes with a predicted tail-first substrate entry will specifically oxygenate not only the free fatty acid substrate but also very large esters such as 1-palmitoyl-2-linoleoylphosphatidylcholine. Furthermore, 5-LOX and 8*S*-LOX, predicted head-first enzymes, have not been found to specifically oxygenate large esters.

There are, however, notable exceptions that challenge the idea implicit in the boot-shaped cavity model that the channel penetrates deep into the protein core. The plant 9-LOX enzymes are predicted to bind substrate in the reversed orientation with respect to 13-LOX and 15-LOX enzymes. Because the 13-LOX and 15-LOX enzymes all successfully oxygenate very large esters [phosphatidylcholine (PC), etc.], in their case it is safe to place the PC moiety "outside" the protein core during catalysis, and thus, it should be "inside" for plant 9-LOX and like enzymes. Clearly, this would be hard to accommodate, and accordingly, one would predict "no reaction". However, plant 9-LOX enzymes do successfully metabolize some bulky esters and amides, for example, anandamide (an ethanolamide moiety) and 1-glycerol linoleate (*35*, *36*). These facts are more readily reconciled with a U-shaped substrate binding mode in which (it is predicted) the ester/amide moiety of these substrates lies outside the protein core at the other end of the channel.

A New Light on R versus S Stereocontrol. One turn of the helix removed from L432 is G428, the amino acid that confers *R* stereochemistry on the 8*R*-LOX product according to Coffa and Brash (*37*). Their observation that a Gly to Ala mutation at this position results in an enzyme that produces the 12*S* product can be explained in the context of the U-shaped channel. Recall that in our model AA is positioned with its carboxyl at R183 (Figure 3) and L432 restrains the pentadiene at the Fe. As a consequence of its role in positioning the pentadiene for attack, L432 is also poised to shield the pentadiene with respect to oxygenation. The wild-type enzyme produces exclusively the 8*R* product; thus, L432 shields C12 from oxygenation. The presence of a C_β at residue 428, however, would serve to push L432 away from C12 and result in the leucine shielding C8 instead. In

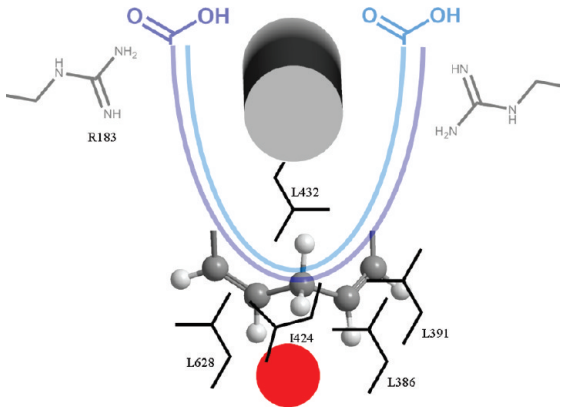

FIGURE 7: Schematic of active site features common to lipoxygenases. Invariant Leu and Ile side chains (black stick) position the pentadiene (ball-and-stick rendering) for attack (numbered according to 8*R*-LOX). An invariant Leu (L432, replaced with Ala, Val, Ile, and Phe) is donated by the arched helix that defines the roof of the active site. The Leu is positioned to clamp the substrate in place above the Fe (red sphere). The direction (and register) of the substrate is set by a neutralizing amino acid (R183 in the 8*R* enzyme) at one of the two ends of the channel.

contrast, in the context of the boot-shaped cavity, the Gly−Ala switch presents a paradox. How does the presence of the methyl group of Ala in the *R*-oxygen pocket (which is more superficial in the boot-shaped cavity) redirect O_2 to a pocket at the *S* position of a pentadiene (*37*, *38*), which would lie deeper in the protein, past the catalytic iron? In the U-shaped channel, the Ala−Gly switch is centrally positioned (i.e., there is a single O_2 pocket) where it can potentially influence either side of the reacting pentadiene and, thus, direct the oxygen molecule to the *R* or *S* position.

Concluding Remarks: A "General" Model for Substrate Binding. Taken together, the high-resolution structure of 8*R*-lipoxygenase from *P. homomalla*, analysis of the impact of mutations on enzyme activity, and data in the literature suggest a general model for substrate binding to lipoxygenases in a U-shaped channel (Figure 7). U-Shaped channels have been proposed to bind the substrate of other fatty acid metabolizing enzymes: the Δ^9-stearoyl-acyl carrier protein desaturase (*39*) and soluble epoxide hydrolase (*40*).

The essential feature of our model is that a conserved arched helix curves over a U-shaped channel lined with invariant leucines and isoleucines. The substrate can slide into this channel and wrap around the arched helix, positioning the central carbon of a pentadiene above the catalytic iron. The conserved Leu and Ile side chains serve to guide and/or clamp the substrate in place, and the Gly−Ala switch is positioned such that only a single oxygen pocket is required. The LOX enzymes that utilize arachidonic acid must discriminate among three chemically equivalent carbons. The amino acids that set the register and thus determine which pentadiene is attacked are on the periphery of the U-shaped channel and would not be expected to be conserved among lipoxygenases catalyzing different regiospecific reactions.

Although the U-shaped channel in 8*R*-LOX is open at both ends, this need not be the case in other LOX. We predict each lipoxygenase isoform is defined by a single site of entry and that the channel either is closed at the opposite end or lacks an appropriately positioned side chain to tether the carboxylate of the substrate. The strict regio- and stereospecificities of the LOX family members can be explained is this structural context.

For either of the two possible orientations, the substrate carboxylate would be solvent-exposed, circumventing the dilemma of "burying a charge" inherent in earlier models (*41*, *42*). In summary, the discovery of the U-shaped channel in 8*R*-LOX has allowed us to present a new concept with regard to substrate binding, one that is open to further evaluation in any of the lipoxygenase enzymes.

ACKNOWLEDGMENT

We thank Cory LaCrouts and Maria Waight for their expert technical assistance. Diffraction data used in this publication were collected at the Gulf Coast Protein Crystallography (GCPCC) Beamline at the Center for Advanced Microstructures and Devices (CAMD). This beamline is supported by National Science Foundation Grant DBI-9871464 with cofunding from the National Institute for General Medical Sciences (NIGMS).

SUPPORTING INFORMATION AVAILABLE

Product analysis by HPLC (Figure S1), representative chromatograms of HETE isomers, sequence alignment of 8*R*-LOX, human 5-lipoxygenase, rabbit reticulocyte 15-LOX, and lipoxygenases from *Arabidopsis* and soybean (S2). This material is available free of charge via the Internet at http://pubs.acs.org.

REFERENCES

1. Brash, A. R. (1999) Lipoxygenases: Occurrence, functions, catalysis, and acquisition of substrate. *J. Biol. Chem. 274*, 23679–23682.
2. Kuhn, H., and Thiele, B. J. (1999) The diversity of the lipoxygenase family. Many sequence data but little information on biological significance. *FEBS Lett. 449*, 7–11.
3. Werz, O., and Steinhilber, D. (2006) Therapeutic options for 5-lipoxygenase inhibitors. *Pharmacol. Ther. 112*, 701–718.
4. Dahlen, S. E. (2006) Treatment of asthma with antileukotrienes: First line or last resort therapy? *Eur. J. Pharmacol. 533*, 40–56.
5. Schneider, C., Pratt, D. A., Porter, N. A., and Brash, A. R. (2007) Control of oxygenation in lipoxygenase and cyclooxygenase catalysis. *Chem. Biol. 14*, 473–488.
6. Neau, D. B., Gilbert, N. C., Bartlett, S. G., Dassey, A., and Newcomer, M. E. (2007) Improving protein crystal quality by selective removal of a Ca^{2+}-dependent membrane-insertion loop. *Acta Crystallogr. F63*, 972–975.
7. Otwinowski, Z., and Minor, W. (1997) Processing of X-ray Diffraction Data Collected in Oscillation Mode. In Methods in Enzymology (Carter, C. W., Jr., and Sweet, R. M., Eds.) pp 307−326, Academic Press, New York.
8. Oldham, M. L., Brash, A. R., and Newcomer, M. E. (2005) Insights from the X-ray crystal structure of coral 8R-lipoxygenase: Calcium activation via A C2-like domain and a structural basis of product chirality. *J. Biol. Chem. 280*, 39545–39552.
9. Emsley, P., and Cowtan, K. (2004) Coot: Model-building tools for molecular graphics. *Acta Crystallogr. D60*, 2126–2132.
10. Collaborative Computational Project (1994) The CCP4 Suite: Programs for Protein Crystallography. *Acta Crystallogr. D50*, 760–763.
11. Zwart, P. H., Afonine, P. V., Grosse-Kunstleve, R. W., Hung, L. W., Ioerger, T. R., McCoy, A. J., McKee, E., Moriarty, N. W., Read, R. J., Sacchettini, J. C., Sauter, N. K., Storoni, L. C., Terwilliger, T. C., and Adams, P. D. (2008) Automated structure solution with the PHENIX suite. *Methods Mol. Biol. 426*, 419–435.
12. Davis, I. W., Leaver-Fay, A., Chen, V. B., Block, J. N., Kapral, G. J., Wang, X., Murray, L. W., Arendall, W. B.III, Snoeyink, J., Richardson, J. S., and Richardson, D. C. (2007) MolProbity: All-atom contacts and structure validation for proteins and nucleic acids. *Nucleic Acids Res. 35*, W375–W383.
13. Boutaud, O., and Brash, A. R. (1999) Purification and catalytic activities of the two domains of the allene oxide synthase-lipoxygenase fusion protein of the coral *Plexaura homomalla*. *J. Biol. Chem. 274*, 33764–33770.
14. Boeglin, W. E., Itoh, A., Zheng, Y., Coffa, G., Howe, G. A., and Brash, A. R. (2008) Investigation of substrate binding and product stereochemistry issues in two linoleate 9-lipoxygenases. *Lipids 43*, 979–987.
15. Schneider, C., Boeglin, W. E., and Brash, A. R. (2000) Enantiomeric separation of hydroxy eicosanoids by chiral column chromatography: Effect of the alcohol modifier. *Anal. Biochem. 287*, 186–189.
16. Boyington, J. C., Gaffney, B. J., and Amzel, L. M. (1993) The three-dimensional structure of an arachidonic acid 15-lipoxygenase. *Science 260*, 1482–1486.
17. Minor, W., Steczko, J., Stec, B., Otwinowski, Z., Bolin, J. T., Walter, R., and Axelrod, B. (1996) Crystal structure of soybean lipoxygenase L-1 at 1.4 Å resolution. *Biochemistry 35*, 10687–10701.
18. Gillmor, S. A., Villasenor, A., Fletterick, R., Sigal, E., and Browner, M. F. (1997) The structure of mammalian 15-lipoxygenase reveals similarity to the lipases and the determinants of substrate specificity. *Nat. Struct. Biol. 4*, 1003–1009 [erratum (1998) *Nat. Struct. Biol. 5* (3), 242].
19. Skrzypczak-Jankun, E., Amzel, L. M., Kroa, B. A., and Funk, M. O. (1997) Structure of soybean lipoxygenase L3 and a comparison with its L1 isoenzyme. *Proteins: Struct., Funct., Genet. 29*, 15–31.
20. Youn, B., Sellhorn, G. E., Mirchel, R. J., Gaffney, B. J., Grimes, H. D., and Kang, C. (2006) Crystal structures of vegetative soybean lipoxygenase VLX-B and VLX-D, and comparisons with seed isoforms LOX-1 and LOX-3. *Proteins 65*, 1008–1020.
21. Choi, J., Chon, J. K., Kim, S., and Shin, W. (2008) Conformational flexibility in mammalian 15S-lipoxygenase: Reinterpretation of the crystallographic data. *Proteins 70*, 1023–1032.
22. Lichtarge, O., and Sowa, M. E. (2002) Evolutionary predictions of binding surfaces and interactions. *Curr. Opin. Struct. Biol. 12*, 21–27.
23. Madabushi, S., Yao, H., Marsh, M., Kristensen, D. M., Philippi, A., Sowa, M. E., and Lichtarge, O. (2002) Structural clusters of evolutionary trace residues are statistically significant and common in proteins. *J. Mol. Biol. 316*, 139–154.
24. Yao, H., Kristensen, D. M., Mihalek, I., Sowa, M. E., Shaw, C., Kimmel, M., Kavraki, L., and Lichtarge, O. (2003) An accurate, sensitive, and scalable method to identify functional sites in protein structures. *J. Mol. Biol. 326*, 255–261.
25. Borngraber, S., Browner, M., Gillmor, S., Gerth, C., Anton, M., Fletterick, R., and Kuhn, H. (1999) Shape and specificity in mammalian 15-lipoxygenase active site. The functional interplay of sequence determinants for the reaction specificity. *J. Biol. Chem. 274*, 37345–37350.
26. Kuhn, H. (2000) Structural basis for the positional specificity of lipoxygenases. *Prostaglandins Other Lipid Mediators 62*, 255–270.
27. Meruvu, S., Walther, M., Ivanov, I., Hammarstrom, S., Furstenberger, G., Krieg, P., Reddanna, P., and Kuhn, H. (2005) Sequence determinants for the reaction specificity of murine (12R)-lipoxygenase: Targeted substrate modification and site-directed mutagenesis. *J. Biol. Chem. 280*, 36633–36641.
28. Billas, I. M., Iwema, T., Garnier, J. M., Mitschler, A., Rochel, N., and Moras, D. (2003) Structural adaptability in the ligand-binding pocket of the ecdysone hormone receptor. *Nature 426*, 91–96.
29. Romanov, S., Wiesner, R., Myagkova, G., Kuhn, H., and Ivanov, I. (2006) Affinity labeling of the rabbit 12/15-lipoxygenase using azido derivatives of arachidonic acid. *Biochemistry 45*, 3554–3562.
30. Minor, W., Steczko, J., Bolin, J. T., Otwinowski, Z., and Axelrod, B. (1993) Crystallographic determination of the active site iron and its ligands in soybean lipoxygenase L-1. *Biochemistry 32*, 6320–6323.
31. Egmond, M. R., Vliegenthart, J. F., and Boldingh, J. (1972) Stereospecificity of the hydrogen abstraction at carbon atom n-8 in the oxygenation of linoleic acid by lipoxygenases from corn germs and soya beans. *Biochem. Biophys. Res. Commun. 48*, 1055–1060.
32. Knapp, M. J., and Klinman, J. P. (2003) Kinetic studies of oxygen reactivity in soybean lipoxygenase-1. *Biochemistry 42*, 11466–11475.
33. Knapp, M. J., Seebeck, F. P., and Klinman, J. P. (2001) Steric control of oxygenation regiochemistry in soybean lipoxygenase-1. *J. Am. Chem. Soc. 123*, 2931–2932.
34. Meyer, M. P., Tomchick, D. R., and Klinman, J. P. (2008) Enzyme structure and dynamics affect hydrogen tunneling: The impact of a remote side chain (I553) in soybean lipoxygenase-1. *Proc. Natl. Acad. Sci. U.S.A. 105*, 1146–1151.
35. van Zadelhoff, G., Veldink, G. A., and Vliegenthart, J. F. (1998) With anandamide as substrate plant 5-lipoxygenases behave like 11-lipoxygenases. *Biochem. Biophys. Res. Commun. 248*, 33–38.
36. Butovich, I. A., and Reddy, C. C. (2001) Enzyme-catalyzed and enzyme-triggered pathways in dioxygenation of 1-monolinoleoyl-rac-glycerol by potato tuber lipoxygenase. *Biochim. Biophys. Acta 1546*, 379–398.
37. Coffa, G., and Brash, A. R. (2004) A single active site residue directs oxygenation stereospecificity in lipoxygenases: Stereocontrol is linked to the position of oxygenation. *Proc. Natl. Acad. Sci. U.S.A 101*, 15579–15584.

38. Coffa, G., Schneider, C., and Brash, A. R. (2005) A comprehensive model of positional and stereo control in lipoxygenases. *Biochem. Biophys. Res. Commun. 338*, 87–92.
39. Lindqvist, Y., Huang, W., Schneider, G., and Shanklin, J. (1996) Crystal structure of Δ9-stearoyl-acyl carrier protein desaturase from castor seed and its relationship to other di-iron proteins. *EMBO J. 15*, 4081–4092.
40. Argiriadi, M. A., Morisseau, C., Hammock, B. D., and Christianson, D. W. (1999) Detoxification of environmental mutagens and carcinogens: Structure, mechanism, and evolution of liver epoxide hydrolase. *Proc. Natl. Acad. Sci. U.S.A. 96*, 10637–10642.
41. Prigge, S. T., Boyington, J. C., Faig, M., Doctor, K. S., Gaffney, B. J., and Amzel, L. M. (1997) Structure and mechanism of lipoxygenases. *Biochimie 79*, 629–636.
42. Browner, M. F., Gillmor, S. A., and Fletterick, R. (1998) Burying a charge. *Nat. Struct. Biol. 5*, 179.
43. DeLano, W. L. (2002) The PyMOL Molecular Graphics System , DeLano Scientific, San Carlos, CA.
44. Liang, J., Edelsbrunner, H., and Woodward, C. (1998) Anatomy of protein pockets and cavities: Measurement of binding site geometry and implications for ligand design. *Protein Sci. 7*, 1884–1897.